Theoretical Evaluation of Maximum Doping Concentration, Breakdown Voltage and On-state Resistance of Field-Plate Compensated Devices

I. Pawel, R. Siemieniec, M. Born

Infineon Technologies Austria AG, Villach, Austria

Abstract

The idealised on-state resistance vs. breakdown voltage behaviour for field-plate compensated devices is analysed for different impact ionisation models. For small device dimensions, we found a significant deviation from common values of maximum doping concentration due to an overestimated impact ionisation coefficient at higher electric fields. This, in turn, leads to a lower doping density and higher on-state resistance compared to the optimal values.

Keywords: MOSFET, Electric Field, Impact Ionisation, Charge Compensation

INTRODUCTION

Several structures to overcome the unipolar silicon limit have been proposed in recent years. The well-known CoolMOS™ device for example represents super-junction devices, where the n-drift region donors are compensated by acceptors located in p-columns as schematically shown in Fig. 1. Super-junction devices are available for blocking voltages in the range of 500 V to 900 V.

For low-voltage devices, the oxide-bypassed or field-plate structure is more advantageous. Here, an isolated field-plate provides the necessary charges to compensate the drift region donors as illustrated in Fig. 2. The idea here is to divert the electric field lines such that the number of field lines passing through any location is minimized. The deviation of field lines requires additional charges somewhere else to allow field lines in the space-charge region to originate or terminate there. The field-plate provides such compensation charges, hence the name "compensation principle".

The on-state resistance of the device is mainly determined by the doping concentration in the mesa region. The design of such devices cannot be accomplished without sophisticated device simulation tools due to the inherent two-dimensional effects. Nevertheless, analytical models provide a better insight into the nature of the underlying effects and serve as a good starting point for device simulation.

DEVICE STRUCTURE

We shall restrict ourselves to the basic structure as shown in Fig. 3. This device structure, as presented e.g. in [1-4], is referred to as a field-plate structure or as an oxide-bypassed structure.

The main parameters are the uniform doping concentration N_D in the mesa or drift region, the mesa width w, the mesa length L and the oxide thickness t_{ox}. Complete compensation is achieved if the entire mesa region is depleted, that is if the space charge width w_{SC} is half the mesa width.
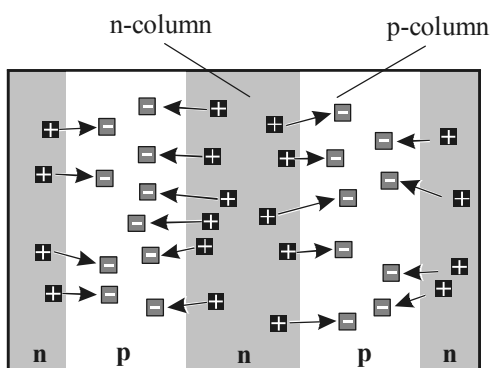

Fig. 1: Compensation of positive donor charges in n-doped columns by negative acceptor charges located in p-doped columns
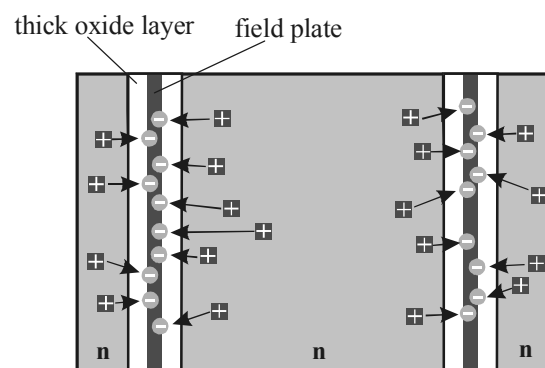

Fig. 2: Compensation of the positive donor charges in the n-region by negative charges located on the isolated field-plates in the trenches
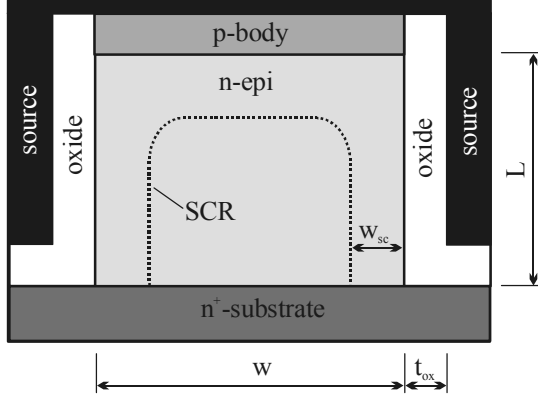
Fig. 3: Basic structure of field-plate compensated devices

IMPACT IONISATION MODELS

The doping in the mesa region determines the on-state resistance and simultaneously the achievable breakdown voltage. To analyse the behaviour of the previously introduced structure, thorough theoretical analysis has been carried out in recent years [4].

Breakdown occurs if the electric field becomes larger than the critical electric field E_{crit}, which depends on the length of the space-charge region (SCR) w_{sc}. $E_{crit} = f(w_{sc})$ is the electric field that causes the ionisation integral to become unity. For electrons, the integral is given by [5]:

$$I_{ava} = \int_0^{w_{sc}} \alpha_n \cdot e^{\int_x^{w_{sc}} (\alpha_p - \alpha_n) \, dx'} \, dx , \qquad (1)$$

where α_n and α_p are the ionisation coefficients for electrons and holes, respectively. A similar expression holds valid for holes:

$$I_{ava} = \int_0^{w_{sc}} \alpha_p \cdot e^{\int_0^x (\alpha_n - \alpha_p) \, dx'} \, dx . \qquad (2)$$

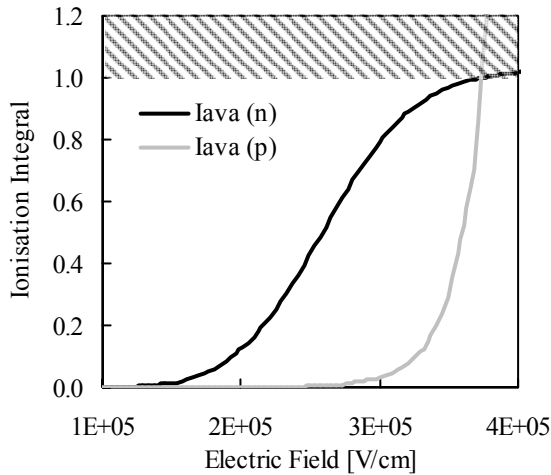Fig. 4 shows the dependence of the ionisation integral

for electrons and holes on the electric field according to the model of Valdinoci [6]. Obviously, the analytic solutions of Eq. 1 and Eq. 2 do not result in equal dependencies. Nevertheless it can be concluded that in case of breakdown the avalanche multiplication of each kind of carrier converges towards an infinite value (e.g. the integral becomes unity). At this point, there is no difference which carrier initiated the process. Consequently, the solution of either Eq. 1 or Eq. 2 is adequate [7,8].

A further simplification is possible if an effective impact ionisation coefficient α_{eff} can be derived. An accurate calculation of the breakdown voltage can be done as long as the relation α_n / α_p is independent of the electric field and thus a constant [9 - 11]. If this assumption is valid in the investigated range of the electric field, the effective impact ionisation coefficient is given by:

$$\alpha_{eff}(E) = \frac{\alpha_n - \alpha_p}{\ln\left(\dfrac{\alpha_n}{\alpha_p}\right)} . \qquad (3)$$

For the ease of calculations, a polynomial approach for the dependency of the effective ionisation coefficient on the electric field E was proposed by Fulop [12]:

$$\alpha(E) = \beta \cdot E^7 . \qquad (4)$$

Eq. 4 is widely used for analytical investigations of power device breakdown capability due to its simplicity. For the expression of Fulop with $\alpha_n \approx \alpha_p \approx \alpha_{eff}$, the avalanche integral reduces to:

$$I_{ava} = \int_0^{w_{sc}} \alpha_{eff} \, dx . \qquad (5)$$

Yet, for smaller device dimensions, this assumed dependency is no longer accurate. Under these conditions, the critical electric field is higher than that predicted by the polynomial approach of Fulop. A better approximation is given in several impact ionisation

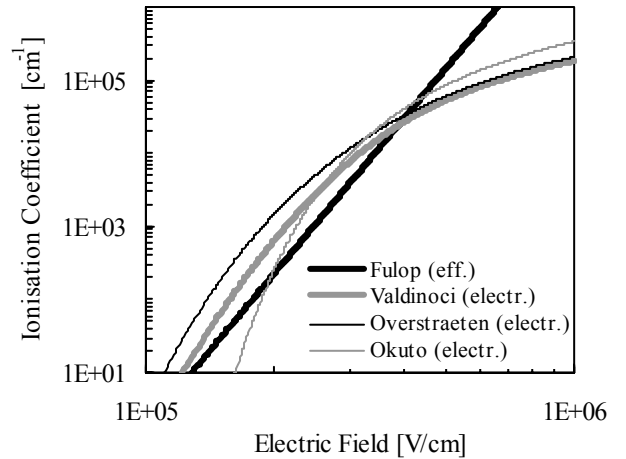Fig. 4: Impact ionisation integral for electron-induced and hole-induced avalanche process

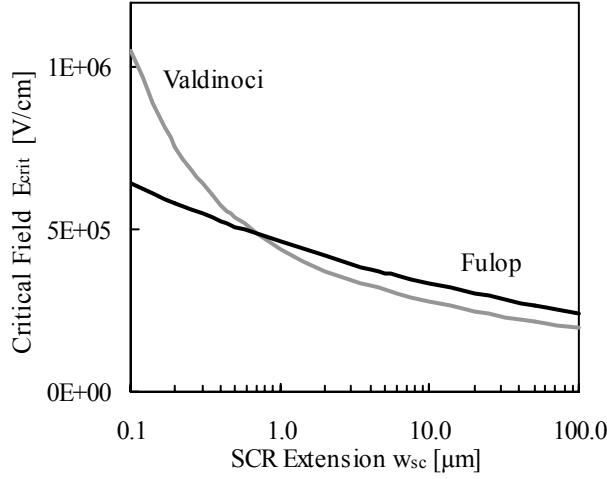Fig. 5: Impact ionisation coefficients as function of the electric field

Fig. 6: Critical electric field as function of ionisation length

models intended to be used in device simulation programs.

A comparison of the effective impact ionisation coefficient α_{eff} as proposed by Fulop [12] and the electron impact ionisation coefficients α_n as given by several impact ionisation models [6,9,13] is provided in Fig. 5. It is clear that Fulop's model differs significantly from these more advanced approaches for electric fields higher than $E = 4 \cdot 10^5$ V/cm.

Instead, the model proposed by Valdinoci [6] is used since it also delivers a better temperature dependency compared to other models [14]. Here, the ionisation coefficients depend on the electric field as follows:

$$\alpha(E) = \frac{E}{a(T) + b(T) \exp \dfrac{d(T)}{E + c(T)}}, \quad (6)$$

with the temperature dependent parameters a,b,c and d.

Application of Eq. 5 to Fulop's model and Eq. 1 to Valdinoci's model is shown in Fig. 6. A significantly higher critical electric field is observed at small dimensions for Valdinoci's model.

Despite the obvious deviations, Fulop's model still is eligible since it allows analytical investigations of impact ionization phenomena while in case of Valdinoci's model a numerical solution is used.

ANALYTICAL MODEL

The 1D- Capacitor

In a first approach, the field-plate oxide stack can be approximated by a capacitor. The voltage across this capacitor is given by:

$$V_{cap} = \frac{Q}{C} = q \cdot N_D \cdot \frac{w}{2} \cdot \frac{t_{ox}}{\varepsilon_0 \cdot \varepsilon_{ox}}, \quad (7)$$

It is assumed that the mesa region is completely depleted by this voltage and that the charge is solely located at the Si/SiO$_2$-interface.

A constant mesa doping gives rise to a triangular horizontal electric field. As a result, the maximum possible voltage drop V_{wsc} in the space-charge region is given by:

$$V_{wsc} = \frac{\varepsilon_0 \cdot \varepsilon_{Si} \cdot E_{crit}^2}{2 \cdot q \cdot N_D}. \quad (8)$$

with the critical electric field E_{crit} for a given doping concentration and space-charge extension w_{sc}.

The applied total voltage V_{total} can be divided into a voltage V_{cap} across the oxide region (capacitor) and a voltage V_{wsc} across the silicon region (mesa) which is important for the breakdown. Their relation can be approximated by a voltage distribution factor:

$$\Theta = \frac{V_{cap}}{V_{wsc}}. \quad (9)$$

Eliminating V_{wsc} gives

$$\Theta = \frac{V_{cap} / V_{total}}{V_{wsc} / V_{total}} = \frac{V_{cap} / V_{total}}{1 - V_{cap} / V_{total}}. \quad (10)$$

The maximum doping concentration in the compensation region can then be obtained from Eq. 7 and Eq. 8 as a function of the critical electric field E_{crit}:

$$N_{D,max} \leq 10^4 \sqrt{\Theta} \frac{\varepsilon_0}{q} \sqrt{\frac{\varepsilon_{Si} \cdot \varepsilon_{ox}}{2}} \cdot \frac{E_{crit}}{\sqrt{\frac{w}{2} t_{ox}}} \text{ cm}^{-3}, \quad (11)$$

with w/2 and t_{ox} in µm, $\varepsilon_0 = 8.85 \cdot 10^{-14}$ F/cm and E_{crit} in V/cm.

From Eq. 11 it can be concluded that in general a higher doping is allowed for smaller device dimensions. It can be seen from Fig. 6, that in case of Valdinoci's model an even larger critical electric field is predicted for decreasing mesa width. For small device dimensions, the higher critical electric field and the smaller
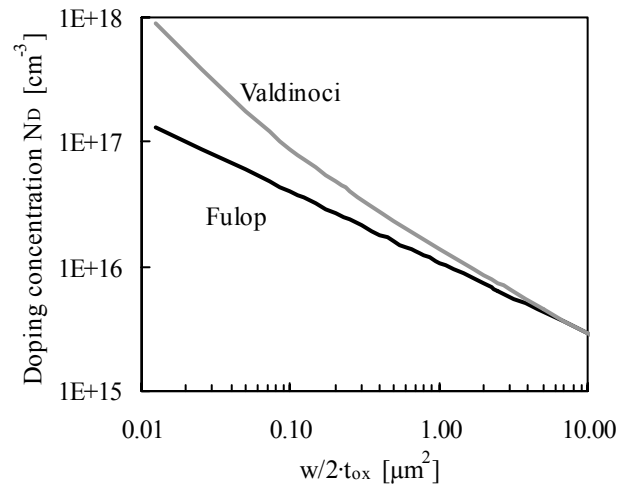

Fig. 7: Comparison of the maximum doping concentration in the drift region for different impact ionisation models as a function of device dimensions ($t_{ox} = 0.5$ µm, $\Theta = 2$)

ionisation coefficient leads to a higher allowed maximum doping density if the model of Valdinoci instead of Fulop is used. This result is shown in Fig. 7. The model employing the impact ionisation rates in accordance with the model of Valdinoci is sufficient to determine the maximum doping concentration which is allowed in the device. Unfortunately, this does not provide any information on the breakdown voltage.

Applying the relation $E_{crit} \propto N_D^{-1/8}$ of [15] to Eq. 11 under the assumption of $\Theta = 1$ gives the well-known relationship derived in [4]:

$$N_{D,max} = 1.07 \cdot 10^{16} \left(\frac{w}{2} t_{ox} \right)^{-\frac{4}{7}} cm^{-3} , \qquad (12)$$

with w/2 and t_{ox} in μm.

The 1D - Field-Plate - MOS System

A more sophisticated model of the structure can be seen in Fig. 8. It generally resembles a simple MOS capacitor, with the exception that no inversion layer can build up because any mobile carriers are removed by the electric field component parallel to the interface. This is taken into account in the capacitor model in Fig. 8 by considering the fixed space charges only, thereby permitting a simple derivation of the electrostatic potential φ and the electric field E.

The latter is constant in the oxide:

$$E_{ox} = \frac{\varphi(0)}{t_{ox}} . \qquad (13)$$

The electric field in the silicon at the Si/SiO$_2$ interface is, with $\eta = \varepsilon_{ox} / \varepsilon_{Si}$ (neglecting interface charges):

$$E(0) = \eta \cdot E_{ox} \qquad (14)$$

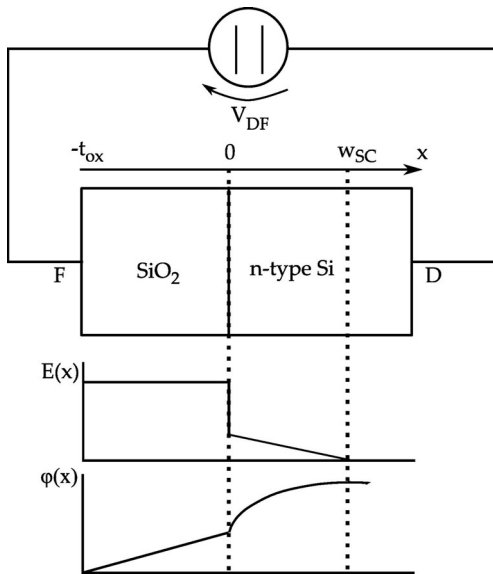Incorporating the additional boundary condition

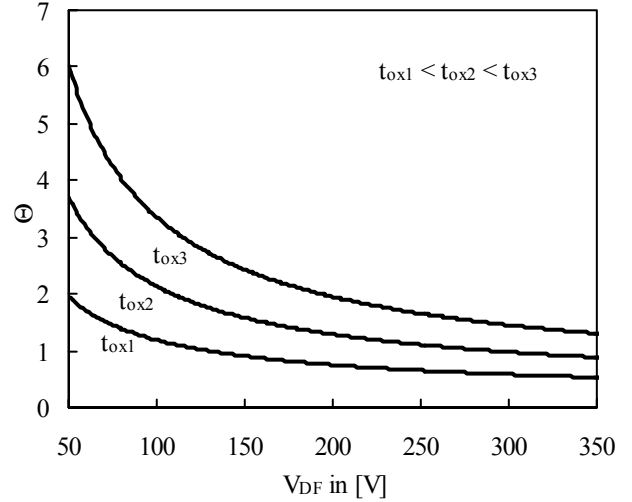
Fig. 8: The MOS-System modelling the field-plate structure

Fig. 9: Voltage distribution factor Θ versus applied drain voltage of the MOS system with constant doping in which V_{DF} is the applied voltage between Drain (D) and field-plate (F).

$$E(w_{SC}) = 0 \qquad (15)$$

into Poisson's equation for the given system leads to the electric field in the silicon

$$E(x) = -\frac{q N_D}{\varepsilon_0 \varepsilon_{Si}} x + \eta \frac{\varphi(0)}{t_{OX}} , \qquad (16)$$

and the length of the space charge region

$$w_{SC} = \eta \frac{\varphi(0)}{t_{OX}} \cdot \frac{\varepsilon_0 \varepsilon_{Si}}{q N_D} . \qquad (17)$$

Note the dependence on φ(0) which is obtained by integrating Eq. 16:

$$\varphi(0) = \frac{-1 + \sqrt{1 + 2 \cdot \xi \cdot V_{DF}}}{\xi} , \qquad (18)$$

with

$$\xi = \frac{\varepsilon_0 \cdot \varepsilon_{Si} \cdot \eta^2}{t_{ox}^2 \cdot q \cdot N_D} \qquad (19)$$

and the voltage between Drain and field-plate V_{DF}. Combining Eq. 17 - 19 finally gives:

$$w_{SC} = \frac{t_{ox}}{\eta} \left(-1 + \sqrt{1 + \frac{2 \cdot \varepsilon_0 \cdot \varepsilon_{Si} \cdot \eta^2}{t_{ox}^2 \cdot q \cdot N_D} V_{DF}} \right) . \qquad (20)$$

With these findings, Eq. 10 translates to

$$\Theta = \frac{\varphi(0) / V_{DF}}{1 - \varphi(0) / V_{DF}} . \qquad (21)$$

A corresponding example plot for one doping concentration value and different oxide thicknesses in the range of interest can be seen in Fig. 9. It shows that the assumption of a constant voltage distribution

factor Θ should be restricted to a sufficiently small voltage range. Under this condition, a carefully chosen value of the voltage distribution factor Θ allows a good estimation of the maximum doping concentration N_D using Eq. 11.

Calculation of breakdown voltage and drift resistance

Within a certain compensation length, the breakdown voltage remains constant [4]. The breakdown voltage in this case depends solely on the mesa width and the critical electric field according to Fig. 6:

$$V_{BD} = 1.8 \cdot 10^{-4} \cdot E_{crit} \left(\frac{w}{2} \right) \cdot \frac{w}{2} \text{ V}, \qquad (22)$$

with E_{crit} in V/cm and w in µm [4].

The device dimensions and doping concentration determine the normalised on-state resistance of the drift zone $R_{Drift} \cdot A$ with length L. It is given by:

$$R_{Drift} \cdot A = \frac{L}{q \cdot \mu_n(N_D) \cdot N_D} \left(1 + \frac{t_{ox}}{w/2} + \frac{t_{FP}/2}{w/2} \right), \quad (23)$$

with the doping dependent electron mobility μ_n and the thickness of the field-plate t_{FP}. A higher doping concentration leads to a lower on-state resistance. However, mobility reduction sets in above a certain doping concentration. The doping concentration can be estimated by using Eq. 11 with a voltage distribution factor $\Theta = 2$:

$$N_D = 10^4 \frac{\varepsilon_0}{q} \sqrt{2} \sqrt{\frac{\varepsilon_{Si} \cdot \varepsilon_{ox}}{2}} \cdot \frac{E_{crit}}{\sqrt{\frac{w}{2} t_{ox}}} \text{ cm}^{-3} . \quad (24)$$

In order to analytically determine the drift resistance R_{Drift}, the minimal drift region length as found in [4], $L = 5 \cdot w/2$, is used. This makes it possible to relate the drift region resistance to the breakdown voltage V_{BD}.

DEVICE SIMULATION

The simulation result of the dependency of the breakdown voltage V_{BD} on the drift region doping N_D for a given structure is shown in Fig. 10. Obviously, there is a maximum doping density leading to a maximum breakdown voltage V_{BD}. Two regions can be distinguished. For doping concentrations to the left of the maximum, the breakdown is mainly pinned at the trench bottom, whereas for doping concentrations to the right of the maximum, the breakdown is located in the middle of the cell. The current paths are different in both cases. This can be seen from breakdown simulations as shown in Fig. 11. The avalanche breakdown location changes if the mesa region is not fully depleted at breakdown. This is the case on the right side of the maximum of the dependency shown in Fig. 10 (e. g. for large doping concentrations). The
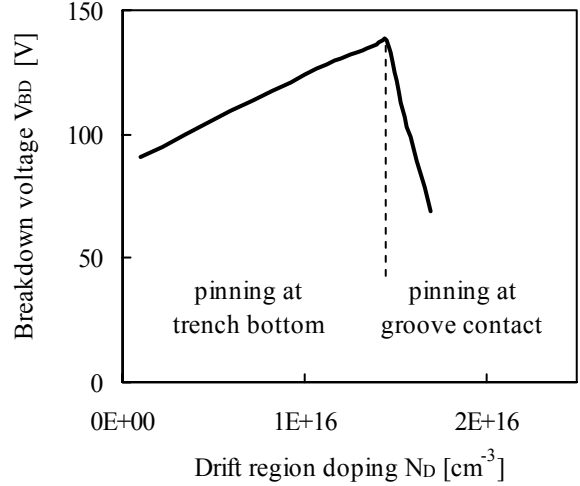

Fig. 10: Simulated characteristics of breakdown voltage as function of drift region doping for a given structure.

increased doping in this region causes the potential to penetrate deep into the mesa region towards the groove contact. The curvature of the equipotential lines is proportional to the doping concentration in the mesa region. If the doping concentration becomes too high, the width of the SCR reduces and drops below half the mesa width. If this happens, any small additional reduction will move the potential lines deeper into the mesa region and the field-plates will increasingly lose their ability to laterally compensate the mesa region. The breakdown voltage V_{BD} further depends on the
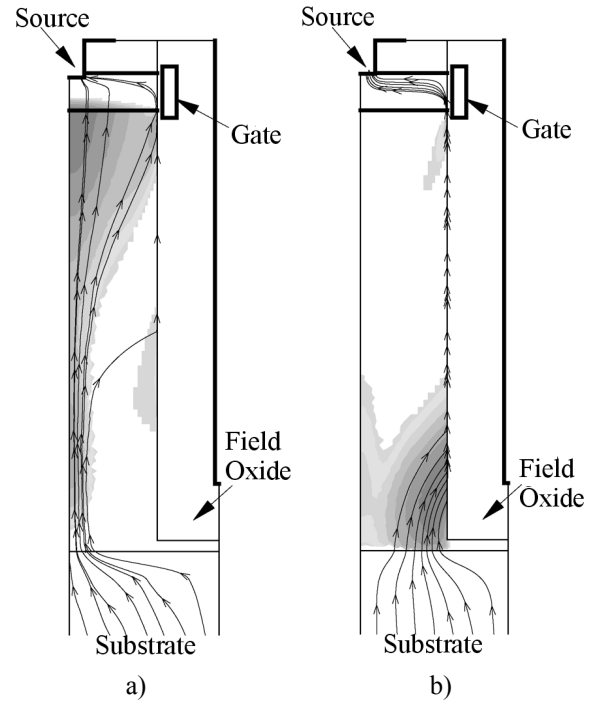

Fig. 11: Location of breakdown for
a) high doping of drift region (right side of maximum)
b) low doping of drift region (left side of maximum)
Contours are impact ionisation rates (dark colours are high values) while the flowlines indicate the current path.
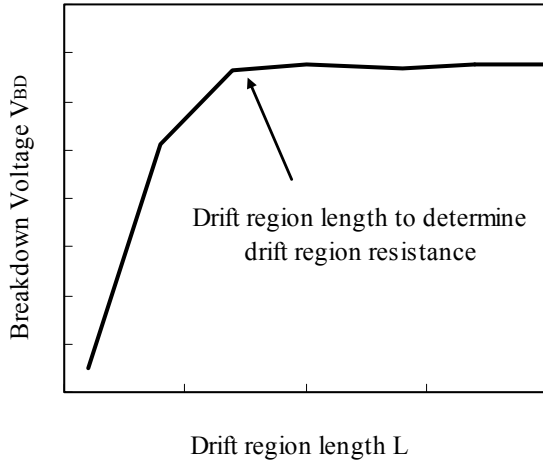
Fig. 12: Determination of drift region length for the calculation of the drift region resistance

Fig. 13: Drift region resistance vs. breakdown voltage for different models

length of the compensation region, i.e. the trench depth [4].

For comparison with the simple analytical model, simulations like the ones shown in Fig. 10 were performed for a large number of structures. Variations included drift region doping N_D, mesa width w, mesa length L and oxide thickness t_{ox} (cf. Fig. 3). Simulations were extended to further investigate the influence of the compensation region length on the breakdown voltage and the drift-region resistance. In a first step, the doping density was varied for a given geometry to find the doping value corresponding to the maximum breakdown voltage. In a second step, the drift region length (and therefore the trench depth) was decreased until the change in the breakdown voltage started to show a significant reduction as qualitatively explained by Fig. 12. Thus for each given geometry, determined by a oxide thickness t_{ox} and a mesa width w, a maximum breakdown voltage V_{BD} and an optimal drift region length L with its corresponding drift region resistance R_{Drift} is found.

In all simulations, the thickness of the field-plate t_{FP} was kept constant.

RESULTS AND COMPARISON

Fig. 13 shows the dependence of the drift region resistance on the maximum gained breakdown voltage. Here, a comparison is given between:

- the model introduced in this work
- the relation found by Chen in [4]
- the 2D simulation results
- the 1D silicon limit [16]

Considering a more realistic dependence of the critical electric field on small dimensions obviously leads to a considerably smaller drift region resistance in comparison with the model presented in [4]. In contrast to these results it can now be concluded that field-plate compensated structures are also an advantageous 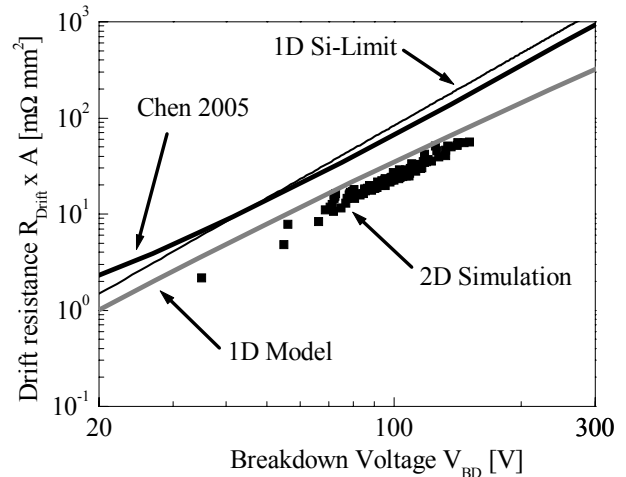alternative for low-voltage devices. This result of the simple 1D model is also supported by the 2D simulation results. Here, even lower values for the drift region resistance are found.

CONCLUSION

For power MOSFETs in the voltage range below 300 V, the application of charge compensation principles leads to structures employing field-plates. These field-plate or oxide-bypassed structures allow the unipolar silicon limit to be overcome.

In this work, the relationship between breakdown voltage and drift region resistance is analysed for such devices. In contrast to similar investigations published elsewhere, a more realistic model for the dependence of the critical electrical field on the ionisation length was considered. This proved to be necessary due to the small device dimensions usually present in the structures of interest and is especially important for devices with low breakdown voltages.

Due to the limitations of the simple 1D model, a voltage distribution factor is introduced. It is shown that this distribution factor is constant within a certain parameter range which allows an estimation of the main parameters of the device.

The results of 2D device simulations, which are not affected by the limitations of the simple 1D model, support the validity of the analytic estimation although lower values of the drift resistance were calculated.

REFERENCES

[1] Liang, Y., Gan, K. and Samudra, G.: Oxide-Bypassed VDMOS (OBVDMOS): An Alternative to Superjunction High Voltage MOS Power Devices, IEEE Electron Device Letters, **22**, 2001, 407-409

[2] Gajda, M., Hodgskiss, S., Mounfield, L. and Irwin, N.: Industrialisation of Resurf Stepped Oxide Technology for Power Transistors, Proc. ISPSD'06 (Naples 2006), 109-112

[3] Pattanayak, D.N., Bai, Y. and Owyang, K.: Low Voltage Super Junction Technology, Proc. ISPS'06 (Prague 2006), 27-36

[4] Chen, Y., Liang, Y. and Samudra, G.: Theoretical Analyses of Oxide-Bypassed Superjunction Power Metal Oxide Semiconductor Field Effect Transistor Devices, Japanese Journal of Applied Physics, **44**, 2005, 847-856

[5] Paul, R.: *Halbleiterphysik*, VEB Verlag Technik Berlin, 1974

[6] Valdinoci, M., Ventura, D., Vecchi, M., Rudan, M., Baccarani, G., Illien, F., Stricker, A. and Zullino, L.: Impact-Ionization in silicon at large operating temperature, Proc. SISPAD'99 (Kyoto 1999), 27-30

[7] Sze, S.M.: Physics *of Semiconductor Devices*, John Wiley & Sons, 1981

[8] Pawel, S.: *Integrierte Gatetreiber für IGBT- und MOS-Leistungssysteme*, Verlag ISLE, 2006

[9] van Overstraeten, R. and de Man, H.: Measurement of the Ionization Rates in Diffused Silicon p-n Junctions, Solid-State Electronics, **13**, 1970, 583-608

[10] Kokosa, R.A. and Davies, R.L.: Avalanche breakdown of diffused silicon p-n Junctions, IEEE Trans. Electron. Devices **ED-13**, 1966, 874-880

[11] Wul, B.M. and Shotov, A.P.: Multiplication of electrons and holes in p-n junctions", Solid State Phys. In Electron. Telecommun., **1**, 1960, 491-497

[12] Fulop, W.: Calculation of Avalanche Breakdown Voltages of Silicon p-n Junctions, Solid-State Electronics, **10**, 1967, 39-43

[13] Okuto, Y. and Crowell, C.: Ionization Coefficients in Semiconductors: A Nonlocal Property, Phys. Rev B, **10**, 1974, 4284-4296

[14] Pawel, I., Siemieniec, R., Rösch, M., Hirler, F. and Herzer, R.: Experimental study and simulations on two different avalanche modes in trench power MOSFETs, IET Circuits, Devices & Systems, **1**, 2007, 341-346

[15] Baliga, B.J.: *Modern Power Devices*, John Wiley & Sons, 1992

[16] Hu, C.: A parametric study of power MOSFETs, Proc. PESC'79 (San Diego 1979), 385-395

Addresses of the authors

Ilja Pawel, Kaiserstrasse 85/1/22, A-1070 Wien, Austria, e-mail: ilja.pawel@web.de

Ralf Siemieniec, Infineon Technologies Austria AG, Siemensstrasse 2, A-9500 Villach, Austria e-mail: ralf.siemieniec@infineon.com

Mathias Born, Infineon Technologies Austria AG, Siemensstrasse 2, A-9500 Villach, Austria e-mail: mathias.born@infineon.com